Virus-host metabolic interactions: using metabolomics to probe oxidative stress, inflammation and systemic immunity

Schoeman, J.C.

Chapter 4

Probing the metabolic innate response of lung epithelial cells upon Respiratory syncytial virus infection

Johannes C. Schoeman, Fatiha Zaaraoui-Boutahar, Ruud Berger, Albert D. M. E. Osterhaus, Thomas Hankemeier, Rob J. Vreeken*, and Arno C. Andeweg*

Manuscript Submitted

* Both authors contributed equally to the manuscript

Abstract

Respiratory Syncytial Virus (RSV) is among the most common causes of hospitalization in infants due to lower respiratory tract infections. The host's immune response to RSV infection is a critical factor in determining disease phenotype, ranging from mild to a life threatening infection. Exploring the RSV-host interaction on the metabolic level remains largely unexplored compared to transcriptome and proteome levels. Oxylipins, known lipid signaling mediators, are involved in the initiation, maintenance and resolution of inflammation. RSV infection of A549 cells, human alveolar epithelial like cells, was used as model to study the role of oxylipins in the innate host response to RSV infection, in a three-day time course study. Using a targeted metabolomics platform for oxylipins, 122 oxylipins were analysed to study the metabolic host response. Transcriptomic analyses targeting oxylipin related genes was performed to complement metabolomics findings. Cyclooxygenase-II oxylipins and related transcripts were identified as early responders to RSV infection, with prostaglandin E_2 & $F_{2\alpha}$ most upregulated within 24 hours post infection. The predominant anti-inflammatory Lipoxygenase and Cytochrome P450 metabolites were characterised with a delayed onset. Collectively the data indicate that RSV has evolved the engineering capacity to interfere and modulate the host's metabolic innate response not only at the synthesis level but also on the catabolic level aiding in RSV propagation. A better understanding of the metabolic pathogenic mechanisms of an RSV infection can help us to understand disease induction and improve therapeutic intervention strategies.

Background

Respiratory Syncytial Virus (RSV), a member of the *Paramyxoviridae* family, is one of the leading causes of lower respiratory tract infection [1,2]. RSV infections may induce varying disease severity in affected individuals, posing a significant threat to infants [1], the elderly [3,4], immunocompromised individuals and patients with underlying chronic disorders [5]. Several risk factors for developing severe RSV disease in infants have been identified, these include preterm birth, RSV viral load and sex, in addition to environmental factors like in-house smoking and concurrent infections [1,6,7]. Since viral strain variation does not appear to play a major role in predicting disease severity [8] the hosts' response is an important determinant of disease severity [8,9]. Understanding the induction and regulatory aspects of the host response to RSV infection is important for understanding pathogenesis, predicting disease severity and for the rational design of effective antiviral strategies.

RSV is a largely airborne transmitted virus with the first site of infection being the upper respiratory tract, spreading to the lower respiratory tract if not cleared [10]. Upon exposure, RSV enters the cell via fusion with the plasma membrane of respiratory epithelium cells releasing the nucleocapsid into the cytoplasm initiating the infection cycle. The F-protein of the viral envelope as well as viral ssRNA and dsRNAs are known as pathogen associated molecular patterns (PAMPs) and are recognised by Toll like receptor (TLR) -4, -3 and -7 respectively, collectively known as pattern recognition receptors (PRRs). PRR activation commences the pathogen recognition stage, signalling for the start of the innate immune response [11,12]. TLRs activated signalling cascades conclude with the activation of an array of transcription factors including: NF-κB, IRF3, IRF7, JNK, and p38 MAPK [11,13]. Activation of transcription factors regulates the expression of genes associated with immune and inflammatory mediators, as well as antimicrobials [13–15]. In addition to these protein gene expression products it has recently been appreciated that also metabolites and more specifically lipid mediators add to cellular signalling and immune regulation [16,17]. Traditionally, research focuses on characterising the innate and/or adaptive response to RSV at the transcriptome and the proteome level. However, the host response at the metabolic level results in a complementary phenotypic readout and presents a largely unexplored route in characterising host responses upon RSV infection. Cytoplasmic phospholipase A_2 ($cPLA_2$) and inducible Cyclooxygenase-II (COX-II) are NF-κB mediated inflammatory gene products and essential players in oxylipin production, a subgroup of lipid mediators indicated **(see Fig. 4.1)** [18,19]. The oxylipins are a comprehensive group of enzymatically oxidised lipid mediators regulating a wide variety of physiological and pathophysiological responses [20,21] and have been identified as potent signalling molecules in the initiation, maintenance and resolution of inflammation [22]. Prostaglandins are prominent members of the oxylipins, with Prostaglandin E_2 previously associated with RSV respiratory infection [23,24]. During RSV infection increased levels of PGE_2 are produced and its biological effects range from a pro-inflammatory mediator [25] to an immune suppressor [26], while also correlating to the development of asthma and allergies [27].

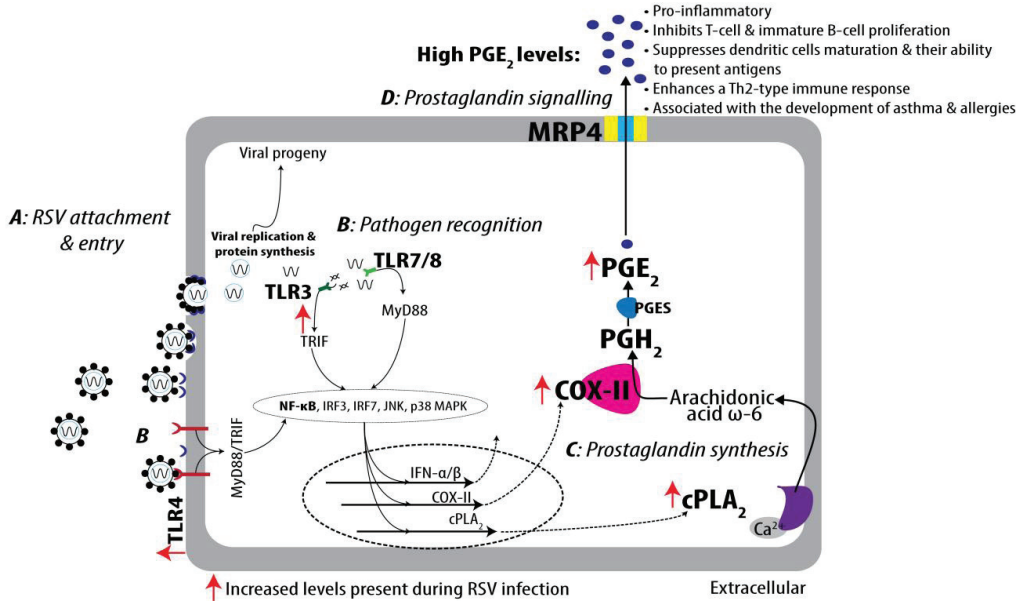

Figure 4:1: Innate immune response activation upon RSV infection and subsequent Prostaglandin E_2 synthesis. (A) RSV attachment and entry. (B) Pathogen recognition. (C) Prostaglandin synthesis: The induced transcription factor NF-κB upregulates the expression of $cPLA_2$ & COX-II, enzymes responsible for the synthesis of eicosanoids and more specifically PGE_2. (D) Prostaglandin signalling**:** After synthesis, PGE_2 is actively secreted from the cell through the ATP dependent MPR-4 transporter. ***PAMPs -*** Pathogen associated molecular patterns, ***PRR -*** Pattern recognition receptors, ***cPLA2*** - cytosolic phospholipase A_2, ***COX-II*** - cyclooxygenase-II, ***MPR-4 -*** Multidrug resistant protein-4, ***PGE_2***- Prostaglandin E_2.

Understanding the initiation, maintenance and regulation of a self-limiting inflammatory response is pivotal in preventing chronic inflammation and tissue damage [28]. This is the first comprehensive *in vitro* viral metabolomics study complimented with a targeted transcriptomics approach to investigate the role of the oxylipins in the innate immune response upon RSV infection. We exploited the A549 cell - RSV A2 *in vitro* infection model and analysed 122 oxylipins during the course of a three-day infection. Oxylipin profiling was used to study the host's innate and inflammatory responses at the metabolic level, and identified the induction of a natural pro-inflammatory innate immune response upon infection. Metabolically the innate immune response was characterised by high levels of PGE_2 and $PGF_{2\alpha}$ within the first 24h. We suggest that RSV has evolved the ability to interfere with, and modulate the host response on the metabolic level contributing to its sustained infection

Methods

Chemicals & reagents

Ultra-performance liquid chromatography (UPLC)-grade acetonitrile, isopropanol, methanol, ethyl-acetate, and water were purchased from Biosolve (the Netherlands). Glacial acetic acid was from Sigma-Aldrich (St. Louis, MO). Oasis HLB (60 mg/30 µm) 96 well plates from Waters (Milford, MA) were used for solid phase extraction (SPE). Deuterated and non-deuterated oxylipin standards were purchased either from Cayman Chemicals (Ann Arbor, MI), Biomol (Plymouth Meeting, PA), or Larodan (Malmö, Sweden).

Cells and viruses

A549 cells were cultured in complete RPMI-1640 medium (Gibco Invitrogen, Carlsbad, CA, USA) supplemented with 5% (v/v) heat-inactivated fetal bovine serum (FBS; Greiner, Frickenhausen, Germany), penicillin (100 U/ml; BioWhittaker), streptomycin (100 µg/ml; BioWhittaker), L-glutamine (2 mM; BioWhittaker) at 37°C and 5% CO2. Molecularly cloned RSV-A2 (a kind gift from A.G.P. Oomens, [29]) was propagated on Vero118 cells at low multiplicity of infection (m.o.i.) and low passage number to avoid generation of defective interfering particles as described by van den Hoogen et al., [30]. Infectivity of the virus stock was measured by serial 10-fold dilutions and the titre was calculated using the method of Reed and Muench [31]. A549 cells were seeded in a 24 well plates at a density of 3×10^6 cells per plate and were allowed to adhere overnight.

Viral infection and TNFα stimulation of A549 cells

Overnight cultures of A549 cells were infected with RSV at a m.o.i. of 3 in serum free medium and incubated at 37°C for 2 hours. At T=0 hour the virus inoculum or serum free medium (mock infection) was removed and replaced by fresh culture media containing 5% fetal bovine serum (FBS). As a positive control, A549 cells were cultured in the presence of TNFα (Peprotech, London, UK) at a concentration of 50 ng/ml. Cell free culture supernatant was collected at T = 0, 12, 24, 36, 48 & 72 hours' post (mock) infection or start of incubation with TNFα. Concurrently viable cell counts per well were taken. Each sample was plated in quadruplicate, and 500 µL from each replicate was collected and pooled to make a total sample volume of 2 mL, 0.8 mg butylated hydroxytoluene (BHT)/EDTA was immediate added before storage at −80 °C prior to eicosanoid extraction. The infection level was determined between 80 to 82 % after 48 h by FACS analysis [32].

Transcriptomic data analyses

Trizol homogenates from an independent A549 RSV infection experiment [33] were processed according to the manufacturer's instructions (Invitrogen life technologies, Carlsbad, CA, USA). Total RNA was isolated and purified using the RNeasy Mini kit (Qiagen, Hilden, Germany): 250 µl of ethanol was added to the upper aqueous phase of the processed Trizol samples and directly transferred to the RNeasy spin columns for purification. RNA concentrations and OD 260/280 nm ratios were measured with the NanoDrop® ND-1000 UV-VIS spectrophotometer (NanoDrop Technologies, Wilmington, USA). Assessment of total RNA quality and purity was performed with the RNA 6000 Nano assay on the Agilent 2100 bioanalyzer (Agilent

Technologies, Palo Alto, CA, USA). cDNA was synthesized from 2 µg total RNA using the One-Cycle Target Labelling kit (Affymetrix, Santa Clara, CA, USA). Biotin-labelled cRNA synthesis, purification and fragmentation were performed according to standard protocols. Fragmented biotinylated cRNA was subsequently hybridised onto Affymetrix Human Genome U133 Plus 2.0 microarray chips, which were scanned with the Affymetrix GeneChip Scanner 7G. A full analysis of these experiments will be described in a later publication.

Oxylipin extraction

Eicosanoid analysis was based on the method of Strassburg et al., 2012 [34]. Briefly, the 2 mL culture medium samples were thawed on ice, aliquoted to 1.5 mL and spiked with 5 µL of deuterated internal standards (ISTDs). Samples were diluted to 6 mL with a 5% MeOH, 0.1 % Acetic acid solution. Solid phase extraction was performed using Oasis HLB (60 mg/30 µm). Oxylipins were eluted with 1.5 mL ethyl acetate after wetting the cartridge with 0.3 mL methanol. The extract was dried under a stream of nitrogen, and reconstituted in 50 µL solution of methanol and acetonitrile (1:1) containing 100 nM 1-cyclohexyluriedo-3-dodecanoic acid (CUDA) functioning as a quality marker for the analysis. Particles were removed by centrifugation filtration using Amicon Ultrafree-MC Durapore PVDF filter (pore-size 0.1 µM; Millipore, Bedford, MA).

Liquid chromatography – Tandem mass spectrometry

Liquid chromatography coupled with Mass spectrometry was done as explained in Strassburg et al 2012 [34]. In short: eicosanoid analysis was performed by liquid chromatography (Agilent 1260, San Jose, CA, USA) coupled to electrospray ionization on a triple quadrupole mass spectrometer (Agilent 6460, San Jose, CA, USA). Chromatographic separations were achieved using an Ascentis Express (2.1×150 mm, 2.7 µm particles; Sigma-Aldrich Supelco) column with a flow rate of 0.35 mL/min at 40 °C. Five µl of the original 50 µl of the sample extract was injected onto the LC–ESI-MS/MS, and separated during a 26 min gradient run. Mobile phase A consisted of 0.1 % acetic acid, and B of 90:10 v/v acetonitrile/isopropanol, with initial conditions set at 15 % B with a step wise increases till 95% B in 19.5 mins. To detect the individual oxylipins, MRM in negative ion mode was performed with a method which makes use of individually optimized fragmentor voltage and collision energies (Optimizer application, Mass-Hunter, Agilent). The detailed list of MRM transitions can be found in the Electronic Supplementary Material Table S-1 of Strassburg et al., 2012 [34].

Quality control samples

Quality control (QC) samples were used during the metabolomics analyses for quality assurance purposes. Equal volumes of each study sample were pooled to obtain the QC pool. A set of QC samples were then included during the analyses of the experimental groups, and evenly distributed through the randomized samples prior to LC-MS analyses. Using the QC samples, a quality control approach was applied to include only those metabolites that were accurately measured (S/N >10) and showed an RSD < 30% within the QC samples. Subsequently, the dataset was filtered, where only the target compounds present in 60% or more of the samples within at least one experimental group were taken into account.

Data processing and statistical analyses

Peak determination and peak area integration was performed with Mass Hunter Quan (Agilent, Version B.05.01). The obtained peak areas of targets were corrected using their respective internal standards. Data pre-treatment consisted of zero replacement (replaced by half of the minimum value in the data set) followed by log transformation and auto scaling. MetaboAnalyst 3.0 was used for principal component analysis (PCA) [35]. GraphPad Prism 6 (GraphPad, La Jolla, CA, USA) was used for unpaired t-test analyses, determining statistical significance using the Sidak-Bonferroni method, with $\alpha = 5.00$ %. Enzymatic and non-enzymatic conversion rates were determined through obtaining the ratio between the downstream metabolite and the respective upstream metabolite within each time point, per group.

For transcriptomics, data were log2-transformed and normalized by variance stabilising normalisation (VSN) [36]. Statistically significant differential expression for each probe set was assessed using the Linear Model for MicroArray data (limma) [37] expressed as the fold change in expression between infected and uninfected conditions (False discovery rate cut-off of 0.05).

Results

Induction of innate host response in RSV infected A549 lung epithelial cells

A synchronised RSV infection in A549 cells was achieved with an infection level of approximately 80 % of the cells and the first cytopathic effects noted within 24h post infection. Subtle morphological changes followed, at 36h post infection, by cell detachment and ultimately cell death resulted in decreased cell numbers over time. Culture medium was collected at regular intervals during 72 hours and subjected to oxylipin analysis because of the secretory nature of these metabolites. Detected metabolite levels were normalised to the live cell counts determined for each time point. Cell count based normalisation is the preferred method in experiments where nuclear and DNA integrity is compromised leading to DNA/cell number ratios that differ from the control groups [38]. The 5% FBS used in the A549 cell cultures appeared to contain pre-existing levels of some of the oxylipins, especially LOX and P450 metabolites. Since oxylipin metabolism has a high turnover rate, as demonstrated in our experiments by the immediate reduction of these serum derived oxylipins upon addition of culture media to monolayers of A549 cells, no oxylipin level correction was required. Actually, in our cell culture the oxylipins were quickly absorbed and metabolised and reached equilibrium as the net effect of cellular production and catabolism. The high turnover rate is directly associated with their potent biological signalling capabilities.

Global oxylipin response

Over the course of the RSV infection experiment, 122 lipid species were profiled of which 60 passed the quality control and were considered eligible for statistical analysis. 62 oxylipin metabolites were excluded from the statistical analysis based on the QC procedures, as they were below or near the limit of detection. PCA was performed to investigate the global metabolic trend associated with infection and time (**Figure 4.2**). After 24 hours' differentiation between RSV infected cells, mock infected cells and TNF_{α} stimulated cells are clearly

distinguishable. Principal component 1 (PC1) accounts for 39.8 % of the variance in the dataset and segregated the experimental groups best. PC2 accounts for 16.7 % of the variance and concurs mostly with time. For the mock infected cultures, no clear intragroup separation is seen after 24 hours (**Fig. 4.2**), revealing that an equilibrium has been obtained. Between time points T=0 and T=24 the cells equilibrate to their new environment metabolising the active signalling mediators present in FBS, and in 24 hours' homeostasis is achieved showing little variation in concentration levels for the later time points. The TNF_{α} stimulated cells are considered a positive control and cluster between the mock - and RSV infected groups. TNF_{α} is a known inducer of inflammation albeit its mechanism for activating inflammation is more downstream when compared to RSV infection.

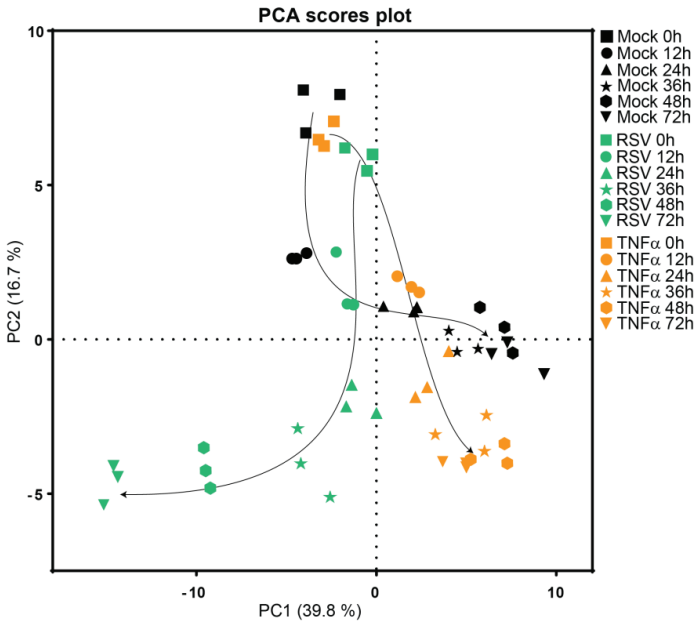

Figure 4.2: PCA score plot. PCA score plots of the normalized culture medium of the RSV infected (green) the positive control (orange - TNF_{α} stimulated) and mock infected (black) groups at the different time points shown in a symbol scale.

Cyclooxygenase Pathway metabolites

The two well described cyclooxygenase isoforms (COX-I/II) are glutathione dependent enzymes responsible for the enzymatic oxidation of poly-unsaturated fatty acids to form the collective group of metabolites known as the Prostaglandins [20]. At 24 hours post infection, prostaglandin levels, especially from the E and F series, were significantly increased based on Sidak-Bonferroni t-tests in the RSV infected group compared to the mock infection. The expression levels of the COX derived oxylipins of which Prostaglandin E_2 and $PGF_{2\alpha}$ were the major prostaglandins produced by the RSV infected cells are shown in **Figure 4.3** as a

heatmap. The COX oxylipins are indicative of a pro-inflammatory response and indeed displayed steadily increasing levels over time upon RSV infection and also upon exposure of the cells to TNFα. The weakest responding COX oxylipins within the RSV infected cells were PGJ_2, Δ^{12}-PGJ_2 and $PGF_{3\alpha}$. The detection of metabolised downstream oxylipins reflected the same trend as their upstream active mediator, confirming their presence [39]. **Supplementary Table S4.1** lists the detected COX derived oxylipins and their respective descriptive statistics. The positive control group showed a weaker but similar trend in both PGE_2 and $PGF_{2\alpha}$ syntheses compared to the RSV group. Prostaglandins E_1, E_3, $F_{1\alpha}$, A_2, 12S-HHTre and 1α,1β-dihomo-$PGF_{2\alpha}$ were nearly exclusively detected in the RSV and positive control groups. Inspecting the relative intra group order of induction of the prostaglandin E_2, $F_{2\alpha}$, and D_2 at 24 and 48 hours, showed for the RSV group: PGE_2 > $PGF_{2\alpha}$ >> PGD_2, for the TNFα group: PGE_2 ≈ $PGF_{2\alpha}$ >> PGD_2 and lastly for the mock group: $PGF_{2\alpha}$ >> PGE_2 > PGD_2 (shown in S**upplementary Figure S4.1**). At the same time the quantitative assessment showed that the highest response changes in the RSV infected cells were observed above the Mock and TNF alpha infected cells.

5-, 12-, 15-Lipooxgenase pathway metabolites

The products of the LOX pathway contain well-defined pro- and anti-inflammatory mediators including: leukotrienes, hydroxyl-fatty acids & lipoxins. The LOX metabolites showed only significant increases 48 hours post infection in the RSV infected cells, in comparison with COX metabolites identified as early as 12h post infection. Sixteen LOX-derived oxylipins from five different poly unsaturated fatty acids (PUFAs) were identified and quantified and are presented in the heatmap in **Figure 4.3**, the relevant descriptive statistics can be found in **Table S4.2.** The strongest LOX responders were 5-, 12-, and 15-hydroxy-eicosatetraenoic acids (HETEs), 5-, 12-, and 15-hydroxy-eicosapentaenoic acids (HEPEs), and two 8- and 15-hydroxyl-eicosatrienoic acids (HETrEs) with arachidonic (20:4 - ω6), eicosapentaenoic (C20:5 - ω3) and eicosatrienoic (C20:3 - ω3) acid being the respective PUFA precursors. 12-HEPE was exclusively detected in the RSV cells in day 2 and day 3. During RSV infection, the LOX oxylipins are characterised by a late/delayed onset. Similar results were found by Dennis et al., (2010) and Tam *et al*., (2013) studying macrophages stimulated *in vitro* with lipopolysaccharide Kdo2-lipid A, and mice infected with different Influenza strains respectively [40,41]. More ω-3 oxylipins were found in the LOX response compared to only a single significant ω-3 COX-II oxylipin namely PGE_3.

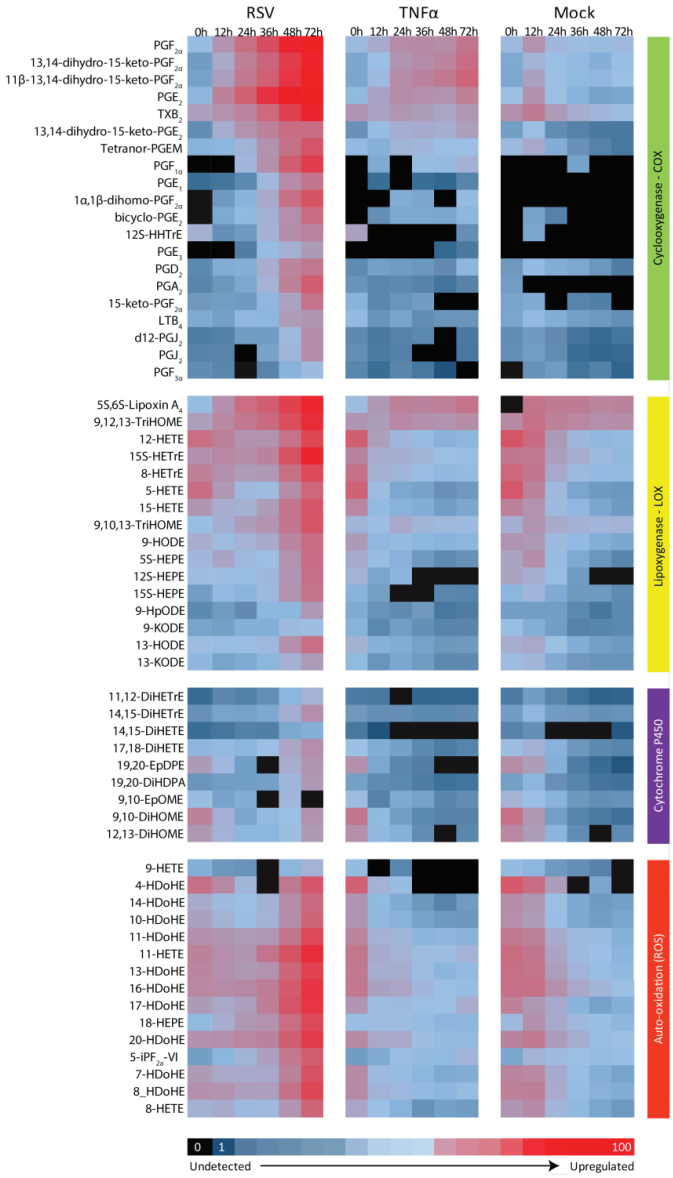

Figure 4.3: Oxylipin profiling heatmap of A549 cells. Detected and quantified oxylipins represented as a heatmap, and divided into the four major synthesis routes COX, LOX, Cytochrome P450, and auto-oxidation. The scaled bar represents the normalised response of all metabolites from undetected to high.

No significant differences were found between the positive and negative control groups; after 72 h at the spiked TNF_α level, no detectable stimulation of the LOX pathway was observed more so then when compared to the mock infection.

Cytochrome P450 Pathway metabolites

Cytochrome P450 enzymes are comprised of a diverse superfamily of P450 isoforms abundantly expressed in the body, with several found in the lungs [42]. The epoxidation of the essential fatty acids by P450's results in the formation of unique bioactive epoxy-lipids [43]. Due to the short half-life of these epoxy-lipids (EETs), in our platform we measure dihydroxy-lipids (DHETs), the stable downstream metabolites. Responses of Cytochrome P-450 metabolites identified are shown in **Figure 4.3 (**and **Table S4.3)**. Oxylipins resulting from the P450 pathway activation was the least provoked during the three-day RSV infection time course. The oxylipins 14,15-dihydroxy-eicosatrienoic acid (DiHETre), 17,18-dihydroxy-eicosatetraenoic acid (DiHETE), 19,20- dihydroxy-docosapentaenoic acid (DiHDPA), together with 9,10- and 12,13- dihydroxy-octadecenoic acid (DiHOME) were found to have subtle increased levels after 2 and 3 days of infection. Again it was found that TNF_α did not lead to a detectable stimulation of the P450 pathway within the allowed 72 hours.

Lipid peroxidation as a read-out for oxidative stress

The ability of RSV infection to modulate and inhibit host antioxidant enzymes links reactive oxygen species (ROS), mediating redox biology, and oxidative stress to inflammation and the immune response [44]. Apart from their role in inflammation, oxylipins also provide a sensitive readout for oxidative stress through the measurement of auto-oxidation species catalysed via reactive oxygen species. In total 15 auto-oxidation oxylipin species (**Figure 4.3 and Table S4.4**) were detected with ten of them derived from docosahexaenoic acid (C22:6 - ω3). The isoprostane 5-i$PF_{2\alpha}$-VI, together with the monohydroxy fatty acids 9-,18-HEPE, and 8-HETE displayed increased concentrations within the RSV group within these 3 days of infection. The hydroxy-docosahexaenoic acid isomers (HDoHEs) identified with increased concentrations in the RSV infected cells, and which are not also associated with an enzymatic pathway included: 4-, 8-, 10-, 11-, 13- 16-, & 20-HDoHE. Low levels of oxidative stress are observed in the negative and positive controls, but with no significant differences between them.

Evaluating the influence of RSV on Prostaglandin metabolism

Extracellular prostaglandin levels are determined through the balance between COX-II synthesising activity and 15-hydroxyprostaglandin dehydrogenase's (15-PGDH) catabolic activity [45]. Consequently, RSV is presented with two opportunities to modulate the host innate prostaglandin response. Prostaglandin catabolism and signal deactivation is primarily achieved enzymatically leading to biologically inactive downstream metabolites and visualised in **Figure S4.2** [46,47]. **Figure 4.4A** indicates the 15-PGDH conversion rate for PGE_2 and $PGF_{2\alpha}$ (active signalling forms) to 13,14-dihydro-15-keto-PGE_2 and 13,14-dihydro-15-keto-$PGF_{2\alpha}$ (deactivated forms) respectively, expressed as the ratio of the downstream metabolite and its active form across the different time points. The positive control group displayed the highest rate of enzymatic signal deactivation. Interestingly, RSV infected cells showed much lower deactivation rates than the mock infection occurring after

24 hours. This demonstrates that during RSV infection PG catabolism is regulated differently compared to healthy dividing control cells and TNF_{α} stimulated cells.

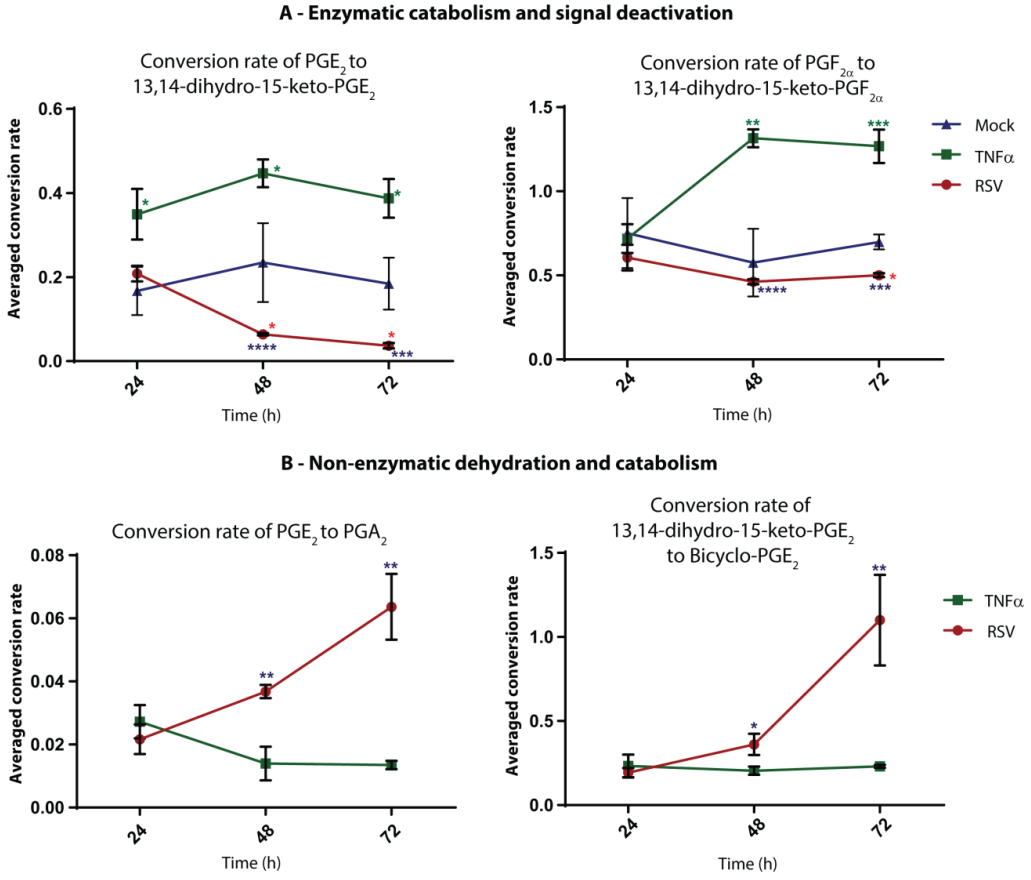

Figure 4.4: A - Enzymatic and B - Non-enzymatic prostaglandin catabolism rates.
Line graphs represent the conversion rate of the active prostaglandin to its downstream metabolite for (A) - Enzymatic and (B) - Non-enzymatic dehydration pathways in the RSV (Red) infected cells, mock (blue) and positive (dark green) control groups respectively. Downstream metabolites were not detected at T = 0 and thus not included in the graphs. The mock was not included in B because PGA_2 and bicyclo-PGE_2 were below the limit of detection within the group. Points on the graphs represent the mean ratio = downstream metabolite / upstream metabolite, with SD as error. The Sidak-Bonferroni method was applied to determine statistical significance (∗0.01< p < 0.05; ∗∗0.001< p < 0.01; ∗∗∗p < 0.001; *****- RSV *vs.* mock, ***** - positive control *vs. mock*, *****- RSV *vs.* positive control.

A secondary route for prostaglandin catabolism occurs non-enzymatically, entailing pH dependent dehydration reactions leading to downstream metabolites, some of which still elicits biological activity (see **Figure S4.2**) [48–50]. The non-enzymatic conversion rate of PGE_2 to the active mediator PGA_2 is shown in **Figure 4.4B**. Initially the conversion of PGE_2 to PGA_2 was similar between RSV infected cells and TNFα stimulated cells, but after 24 hours a statistically significant increase in the rate of PGE_2 dehydration occurs within the RSV group. PGA_2 was not detected in the mock infected group. This finding was also observed in the base favoured decomposition of the inactive 13,14-dihydro-15-keto-PGE_2 to form the stable inert bicycle-PGE_2, which was increased in the RSV group and is a good measure of PGE_2 production [48].

Oxylipin related transcriptomics analyses:

To complement the metabolomics data, we screened 83 oxylipin biosynthesis related genes for differential expression (**Table 4.1**) in an independent A549 RSV infection experiment. Genes related to the COX, LOX and P450 pathways, phospholipases and fatty acid elongation as well as cellular oxylipin receptors and transporters were selected for this analysis. Messenger RNA transcripts were measured at 6, 12 and 24 hours post RSV infection. Eight oxylipin related genes were differentially expressed 24-hour post infection when compared with mock infected control cells. The COX-pathway transcripts *CBR3*, *PTGS2* and the PGE_2 membrane receptor *PTGER4* were found upregulated. Upregulation of *ELOVL7* indicated fatty acid elongation pathway activity and downregulation of *CYP4F3* indicated suppression of the P450 pathway. The phospholipase gene targets indicated differential regulation with upregulation of Ca^{2+}-independent *PLA2G4C* and *PLA1A* and downregulation of Ca^{2+}-dependent *PLA2G12A*. No detectable changes in the gene targets of the LOX-pathway were measured within the first 24h of RSV infection.

Table 4.1: Oxylipin directed transcriptomic gene target list and response during RSV infection.

Targeted Metabolic Pathway (n)	Gene Targets	Upregulated*	Downregulated*
COX pathway (14)	HPGD, **PTGS2,** PTGS1, PTGDS, PTGES, PTGES2, PTGES3, PTGIS, TBXAS1, **CBR3,** CBR1, CBR4, AKR1A1, AKR1C3	CBR3, PTGS2	
LOX pathway (13)	ALOX15B, ALOX5, ALOX12, ALOX15, LTA4H, LTC4S, GPX1, GPX3, GPX2, GPX5, GPX7, GGT6, GGT1		
Cytochrome P450 pathway (15)	CYP1A2, CYP2B6, CYP2C18, CYP2C19, CYP2C8, CYP2C9, CYP2E1, CYP2J2, CYP2U1, CYP4A11, CYP4F11, CYP4F22, **CYP4F3,** CYP4F8, EPHX2		CYP4F3
Phospholipase (20)	PLA2G2E, PLA2G2F, PLA2G3, PLA2G4A, PLA2G4B, **PLA2G4C,** PLA2G4D, PLA2G4E, PLA2G5, PLA2G6, PLA2G7, PLAA, PLB1, **PLA1A,** PLA2G10, **PLA2G12A,** PLA2G12B, PLA2G1B, PLA2G2D, PLA2G2A	PLA2G4C, PLA1A	PLA2G12A
Fatty acid biosynthesis (7)	ELOVL5, ELOVL6, ELOVL2, ELOVL1, ELOVL4, **ELOVL7,** ELOVL3	ELOVL7	
Membrane receptors (12)	PTGFR, PTGIR, PPARA, **PTGER4,** PTGIR, PTGER2, PLA2R1, PPARG, PTGDR, PTGER1, PTGER3, TBXA2R,	PTGER4	
Membrane transporters (2)	ABCC4, SLCO2A1		

*Genes with an absolute fold change (FC) value of > 2 were identified as upregulated and genes with an absolute FC < 0.5 were identified as downregulated respectively (at a false discovery rate of 0.05).

Discussion

A protective host response to RSV is critically dependent on the establishment of a well-balanced immune response initiated locally in the respiratory epithelium. Omics-technologies offer new perspectives on understanding of the virus-host interaction. Here we study the innate response on the metabolic level to RSV infection in lung epithelial cells with a targeted metabolomics approach using a recently developed mass spectrometry based oxylipin analysis platform [34].

The oxylipin profile of RSV infected lung epithelial cells was determined at five time points post infection. Integration of the collected oxylipin metabolite data with data on differentially expressed oxylipin metabolism related gene transcripts results in a oxylipin model at the onset of RSV infection (0-24 h) as depicted in **Figure 4.5**. In this model a calcium-independent phospholipase gene signature is upregulated in response to RSV infection, omitting the need for co-factors and possible inhibitory mechanisms, the gene signature promotes the release of free fatty acids into the cytosol, serving as precursors for oxylipin biosynthesis (see **Fig. 4.5**). Increased intracellular free fatty acid levels also activate the peroxisome proliferator-activated receptor-alpha (PPARα) responsible for homeostatic lipid level regulation, activating amongst others the ELOVL enzyme family [51]. The upregulation of the rate limiting *ELOVL7* within the RSV infected cells trigger the start of long

chain fatty acid elongation [52]. The metabolite, 1α,1β-dihomo-$PGF_{2\alpha}$, is the COX-II pathway product of adrenic acid (C22:4), which in turn is the ELOVL product of a two carbon elongation of arachidonic acid (C20:4), and was found upregulated (see **Fig. 4.3**) within the RSV infected cells supporting this finding [53]. These results reflect the close link between metabolic processes involved in homeostasis and immune signalling.

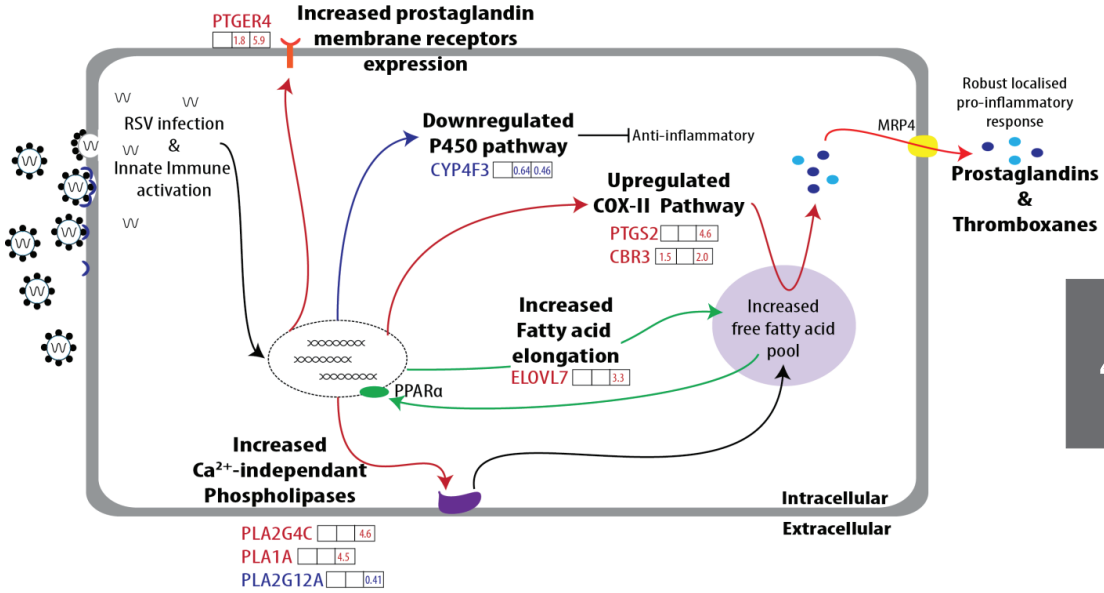

Figure 4.5: Oxylipin model of the first 24 h of a RSV infection. Visualisation of the connection between the metabolic pathway and the differentially expressed oxylipin related gene transcripts. Upregulated phospholipase activity increases the intracellular free fatty acid pool which acts as the substrate during ELOVL dependent fatty acid elongation, as well as for the oxylipin precursors. The log2 fold change values of each gene related to 6, 12 and 24h are presented in boxes next to each significant gene transcript. Red arrows indicate upregulated pathways, blue arrows indicate downregulated pathways, and green arrows indicates cellular consequences.

Both metabolomics and transcriptomics data identified the upregulation of the COX-II pathway within 24h post infection (see **Fig. 4.5**), indicating its central role in the innate immune response. The major prostaglandins produced by the RSV infected cells were PGE_2 followed by $PGF_{2\alpha}$, correlating with the upregulation of the genes *PTGS2* and *CBR3*. These prostaglandins in conjunction with TXA_2 are well-documented pro-inflammatory molecules, playing a beneficial role within the host through inducing a robust inflammatory response leading to acute inflammation at the onset of RSV infection. PGE_2 and $PGF_{2\alpha}$ functions as chemotactic mediators leading to the infiltration of neutrophils, macrophages and mast cells into the affected tissue, additionally, blood flow is also increased via arterial vasodilatory mechanisms at the site of infection [54].

Nevertheless, PGE_2 can be considered as a double-edged sword, as it elicits not only "antiviral" signalling pathways, but also pathways beneficial for sustained RSV infection. Increased expression of *PTGER4* in lung epithelial cells, encoding the PGE_2 membrane bound receptor EP4, could contribute to viral pathogenesis through phosphoinositol-3-kinase (PI3K) signaling cascades [55]. Activation of EP4 and PI3K signaling has been shown to counteract premature apoptosis of infected cells during the later stages of infection, supporting RSV survival [56,57]. Furthermore, high levels of PGE_2 elicit immunomodulatory functions on the infiltrating leukocytes especially macrophages and dendritic cells. PGE_2 can attenuate the macrophage mediated IFN-γ immune response (T_H1 response) while also suppressing apoptosis and the formation of apoptotic vesicles [58]. Antigens, which are important during the cross-talk with T-cells, are present within the apoptotic vesicles and scavenged by dendritic cells (DCs) [59]. In addition, PGE_2 signaling via EP4 within the DCs suppresses its ability to attract naive, memory, and effector T cells. In summary, PGE_2 hinders the switch between innate and adaptive immune responses [26,60]. By inducing the excretion of high PGE_2 levels RSV may exploit these immunosuppressive abilities. As PGE_2 can selectively inhibit the IFN-γ producing T_H1 immune response within macrophages it could skew the immune response towards the less favoured T_H2 regulatory T-cell immune response. RSV infections experiencing a T_H2 immune response is associated with an enhanced and more severe disease profile [61].

Due to the potent biological signalling activity of prostaglandins, fast enzymatic deactivation of the active PG molecules is necessary, which presents a secondary site for RSV interference in the host's response. A strong induction of prostaglandin synthesis was observed in the RSV infected cells, simultaneously, a significant reduced rate of enzymatic prostaglandin deactivation was found compared to the mock and positive control groups as shown in **Figure 4.4 A**. RSV apparently has the ability to upregulate COX II expression and through this evoke a downregulation, direct or indirect, of 15-PGDH activity and prostaglandin deactivation [62]. Due to the transcriptomics experimental time frame of 24 hours, the transcriptomics data could not be used to substantiate this metabolomics finding significantly visible 24h post infection. TNF_α has also been shown to down-regulate 15-PGDH gene expression [63], although the high levels of signal deactivation rates in the positive control group indicates that TNF_α alone is insufficient to have a significant inhibitory effect on prostaglandin silencing. Subsequently, the ability of RSV to downregulate enzymatic prostaglandin silencing via 15-PGDH, ensures high circulating levels of prostaglandin molecules indirectly promoting RSV survival via its immunosuppressive actions, as explained above.

Considering the non-enzymatic prostaglandin catabolism rate, a host beneficial effect was observed. The PGE_2 dehydration rate, and 13,14-dihydro-15-keto-PGE_2 decomposition rate, is pH dependent, with an increase in pH favouring both reactions [48,49]. Significant increases in PGA_2, a spontaneous dehydration product of PGE_2, implies intracellular alkalinisation is occurring during RSV infection which is also a hallmark of apoptosis [64]. Prostaglandin A_2 possess anti-inflammatory and antiviral properties signalling via the PPAR-γ [65–67]. Prostaglandins of the A series affect viral replication by acting at multiple levels including inhibiting viral protein synthesis [68], preventing viral maturation [69], and by inducing the heat-shock protein inhibiting viral replication [68]. In addition, at high concentrations, PGA_2 also has cytotoxic and apoptotic effects; it is able to block the cell cycle progression [70] and directly stimulates the mitochondrial outer membrane permeability to release cytochrome C [71]. The formation of PGA_2 reflects the co-evolution of the host and virus, with the host

able to non-enzymatically regulate the high circulating levels of PGE_2 as it possesses several beneficial antiviral functions for the host.

Oxidative stress is the result of perturbed redox biology, with ROS levels exceeding the antioxidant threshold of the cell, and it has been found that RSV induces oxidative stress by modulating antioxidant enzyme levels [44]. Low levels of ROS help stimulate cell division [72], which also supports viral replication. The increased lipid peroxidation products indicate an imbalance in the cell's antioxidant abilities, highlighting the increased oxidative stress experienced during viral infection [73,74]. Although the non-enzymatic hydroxy-docosahexaenoic acid (HDoHE) isomers are used as an readout for oxidative stress, we detected two specific isomers which can also be synthesised enzymatically via 12- and 15-LOX [75], and have an important biological function; these two isomers 14- & 17-HDoHE identified as increased within the RSV group, are pathway intermediates for Maresins (7-MaR1) and Resolvins (RvD1) respectively, both which are specialized pro-resolving oxylipins [22]. Only after 48h did LOX and P450 metabolites start to appear, supporting the hypothesis of Kuhn and O'Donnell that the LOX genes do not belong to the family of immediate responders to interleukin and cytokine stimulation [76]. Cytochrome P450 derived EETs and LOX derived HODEs are potent anti-inflammatory mediators able to inhibit the NF-kB signalling cascade [77,78]. From the TNF_α stimulated cells no significant time point differences were found between the LOX and P450 metabolites at the spiked TNF_α level. Therefore, the LOX and P450 pathways seem to be governed by factors other than a pure inflammatory response, and the innate immune response. With the late onset of the LOX and P450 pathways, their functions might include the suppression of the early responding pro-inflammatory COX pathway. Enhancing a robust response of these two latter pathways might prove effective in minimising the damage caused by high levels of circulating prostaglandins.

Conclusion

Recently the appreciation of lipid mediators in cellular signalling in the field of immunology and inflammation has been gaining momentum, and integration with more traditional approaches, including transcriptomics and/or proteomics, are presenting us with new ways to study host responses towards viral infections. Upon RSV infection of A549 cells, we identified a calcium-independent upregulated phospholipase signature concurrently with an upregulated COX-II and reduced cytochrome P450 pathway in the host. This natural pro-inflammatory innate response is characterised by high levels of both PGE_2 and $PGF_{2\alpha}$ within the first 24h. In addition, RSV apparently has evolved the ability to interfere and modulate the host's metabolic innate response not only at the synthesis level but also on the enzymatic catabolic level. The preservation of high PGE_2 levels presents RSV with several immunosuppressive and evasive strategies. Although, the resulting increase in PGA_2 elicites multiple antiviral properties and demonstrates the evolution of this virus-host interaction, i.e. how the host can benefit from higher PGE_2 levels, too. The late onset of LOX and P450 metabolites may highlight these pathways as anti-inflammatory regulators opposing the role of COX derived prostaglandins. Individuals predisposed to a strong pro-inflammatory COX-II pathway response, a weak anti-inflammatory LOX / P450 response may experience an oxylipin imbalance potentially contributing to disease severity. Understanding the fine balance between the role of oxylipins in the immune response and RSV ability to exploit the host innate response may contribute in understanding disease progression and ultimately lead to more effective treatment approaches including development of host response modifiers.

Acknowledgements

We thank Katrin Strassburg (LACDR, Analytical Biosciences, Leiden University) for helpful discussions and start up support. A special thanks to Amy C Harms (LACDR, BMFL, Leiden University) for the proof reading and editing of the manuscript. This study was supported by the NWO-ZonMW grant number 435002027, and the Virgo consortium, funded by the Dutch government project number FES0908.

References

1. Nair, H. *et al.* Global burden of acute lower respiratory infections due to respiratory syncytial virus in young children: a systematic review and meta-analysis. *Lancet* **375,** 1545–55 (2010).
2. Simões, E. A. F. *et al.* Challenges and opportunities in developing respiratory syncytial virus therapeutics. *J. Infect. Dis.* **211 Suppl,** S1–S20 (2015).
3. Falsey, A. R. & Walsh, E. E. Respiratory syncytial virus infection in adults. *Clin. Microbiol. Rev.* **13,** 371–84 (2000).
4. Walsh, E. E., Peterson, D. R. & Falsey, A. R. Risk factors for severe respiratory syncytial virus infection in elderly persons. *J. Infect. Dis.* **189,** 233–8 (2004).
5. Hynicka, L. M. & Ensor, C. R. Prophylaxis and treatment of respiratory syncytial virus in adult immunocompromised patients. *Ann. Pharmacother.* **46,** 558–66 (2012).
6. El Saleeby, C. M., Bush, A. J., Harrison, L. M., Aitken, J. A. & Devincenzo, J. P. Respiratory syncytial virus load, viral dynamics, and disease severity in previously healthy naturally infected children. *J. Infect. Dis.* **204,** 996–1002 (2011).
7. Borchers, A. T., Chang, C., Gershwin, M. E. & Gershwin, L. J. Respiratory syncytial virus--a comprehensive review. *Clin. Rev. Allergy Immunol.* **45,** 331–79 (2013).
8. Venter, M., Collinson, M. & Schoub, B. D. Molecular epidemiological analysis of community circulating respiratory syncytial virus in rural South Africa: Comparison of viruses and genotypes responsible for different disease manifestations. *J. Med. Virol.* **68,** 452–61 (2002).
9. Villenave, R. *et al.* Differential cytopathogenesis of respiratory syncytial virus prototypic and clinical isolates in primary pediatric bronchial epithelial cells. *Virol. J.* **8,** 43 (2011).
10. Wright, M. & Piedimonte, G. Respiratory syncytial virus prevention and therapy: past, present, and future. *Pediatr. Pulmonol.* **46,** 324–47 (2011).
11. Oshansky, C. M., Zhang, W., Moore, E. & Tripp, R. A. The host response and molecular pathogenesis associated with respiratory syncytial virus infection. *Future Microbiol.* **4,** 279–297 (2009).
12. Xagorari, A. & Chlichlia, K. Toll-like receptors and viruses: induction of innate antiviral immune responses. *Open Microbiol. J.* **2,** 49–59 (2008).
13. Newton, K. & Dixit, V. M. Signaling in innate immunity and inflammation. *Cold Spring Harb. Perspect. Biol.* **4,** (2012).
14. Akira, S., Uematsu, S. & Takeuchi, O. Pathogen recognition and innate immunity. *Cell* **124,** 783–801 (2006).
15. Jensen, S. & Thomsen, A. R. Sensing of RNA viruses: a review of innate immune receptors involved in recognizing RNA virus invasion. *J. Virol.* **86,** 2900–10 (2012).
16. Norris, P. C., Reichart, D., Dumlao, D. S., Glass, C. K. & Dennis, E. a. Specificity of eicosanoid production depends on the TLR-4-stimulated macrophage phenotype. *J. Leukoc. Biol.* **90,** 563–74 (2011).
17. Stables, M. J. & Gilroy, D. W. Old and new generation lipid mediators in acute inflammation and resolution. *Prog. Lipid Res.* **50,** 35–51 (2011).
18. Steer, S. A. & Corbett, J. A. Viral Infection. **16,** 447–460 (2003).
19. Liu, T. *et al.* RSV-induced prostaglandin E2 production occurs via cPLA2 activation: role in viral replication. *Virology* **343,** 12–24 (2005).

20. Buczynski, M. W., Dumlao, D. S. & Dennis, E. A. Thematic Review Series: Proteomics. An integrated omics analysis of eicosanoid biology. *J. Lipid Res.* **50,** 1015–38 (2009).
21. Quehenberger, O. & Dennis, E. A. The human plasma lipidome. *N. Engl. J. Med.* **365,** 1812–23 (2011).
22. Serhan, C. N. Novel lipid mediators and resolution mechanisms in acute inflammation: to resolve or not? *Am. J. Pathol.* **177,** 1576–91 (2010).
23. Liu, Y. *et al.* The antiinflammatory effect of laminar flow: the role of PPARgamma, epoxyeicosatrienoic acids, and soluble epoxide hydrolase. *Proc. Natl. Acad. Sci. U. S. A.* **102,** 16747–52 (2005).
24. Richardson, J. Y. *et al.* Respiratory syncytial virus (RSV) infection induces cyclooxygenase 2: a potential target for RSV therapy. *J. Immunol.* **174,** 4356–64 (2005).
25. Ricciotti, E. & FitzGerald, G. A. Prostaglandins and Inflammation. *Arterioscler. Thromb. Vasc. Biol.* **31,** 986–1000 (2011).
26. Kalinski, P. Regulation of immune responses by prostaglandin E2. *J. Immunol. (Baltimore, Md 1950)* **188,** 21–28 (2012).
27. Sastre, B. & del Pozo, V. Role of PGE2 in asthma and nonasthmatic eosinophilic bronchitis. *Mediators Inflamm.* **2012,** 645383 (2012).
28. Nathan, C. & Ding, A. Nonresolving inflammation. *Cell* **140,** 871–82 (2010).
29. Oomens, A. G. P., Megaw, A. G. & Wertz, G. W. Infectivity of a human respiratory syncytial virus lacking the SH, G, and F proteins is efficiently mediated by the vesicular stomatitis virus G protein. *J. Virol.* **77,** 3785–98 (2003).
30. van den Hoogen, B. G. *et al.* Excessive production and extreme editing of human metapneumovirus defective interfering RNA is associated with type I IFN induction. *J. Gen. Virol.* **95,** 1625–33 (2014).
31. Reed, L.J. and Muench, H. A simple method of estimating fifty percent endpoints. *Am. J. Hyg.* **27,** 493–7 (1938).
32. Yu, H., Empig, C., Xia, J. & Anderson, W. F. Quantitation of MoMuLV envelope protein on the cell surface. *Virology* **243,** 415–22 (1998).
33. van Diepen, A. *et al.* Quantitative proteome profiling of respiratory virus-infected lung epithelial cells. *J. Proteomics* **73,** 1680–1693 (2010).
34. Strassburg, K. *et al.* Quantitative profiling of oxylipins through comprehensive LC-MS/MS analysis: application in cardiac surgery. *Anal. Bioanal. Chem.* **404,** 1413–26 (2012).
35. Xia, J., Sinelnikov, I. V., Han, B. & Wishart, D. S. MetaboAnalyst 3.0—making metabolomics more meaningful. *Nucleic Acids Res.* **43,** W251–W257 (2015).
36. Pradervand, S. *et al.* Impact of normalization on miRNA microarray expression profiling. *RNA* **15,** 493–501 (2009).
37. Smyth, G. K. Linear models and empirical bayes methods for assessing differential expression in microarray experiments. *Stat. Appl. Genet. Mol. Biol.* **3,** Article3 (2004).
38. Silva, L. P. *et al.* Measurement of DNA concentration as a normalization strategy for metabolomic data from adherent cell lines. *Anal. Chem.* **85,** 9536–9542 (2013).
39. Westlund, P., Kumlin, M., Nordenström, A. & Granström, E. Circulating and urinary thromboxane B2 metabolites in the rabbit: 11-dehydro-thromboxane B2 as parameter of thromboxane production. *Prostaglandins* **31,** 413–43 (1986).
40. Dennis, E. A. *et al.* A mouse macrophage lipidome. *J. Biol. Chem.* **285,** 39976–85 (2010).
41. Tam, V. C. *et al.* Lipidomic Profiling of Influenza Infection Identifies Mediators that Induce and Resolve Inflammation. *Cell* **154,** 213–227 (2013).
42. Jacobs, E. R. & Zeldin, D. C. The lung HETEs (and EETs) up. *Am. J. Physiol. Heart Circ. Physiol.* **280,** H1–H10 (2001).
43. Spector, A. A. Arachidonic acid cytochrome P450 epoxygenase pathway. *J. Lipid Res.* **50 Suppl,** S52-6 (2009).
44. Hosakote, Y. M., Liu, T., Castro, S. M., Garofalo, R. P. & Casola, A. Respiratory syncytial virus induces oxidative stress by modulating antioxidant enzymes. *Am. J. Respir. Cell Mol. Biol.* **41,** 348–57 (2009).
45. Rodriguez, M. & Clare-Salzler, M. Eicosanoid imbalance in the NOD mouse is related to a

dysregulation in soluble epoxide hydrolase and 15-PGDH expression. *Ann. N. Y. Acad. Sci.* **1079,** 130–4 (2006).
46. Tai, H. H., Ensor, C. M., Tong, M., Zhou, H. & Yan, F. Prostaglandin catabolizing enzymes. *Prostaglandins Other Lipid Mediat.* **68–69,** 483–493 (2002).
47. Anggård, E. The biological activities of three metabolites of prostaglandin E 1. *Acta Physiol. Scand.* **66,** 509–10 (1966).
48. Fitzpatrick, F. A., Aguirre, R., Pike, J. E. & Lincoln, F. H. The stability of 13,14-dihydro-15 keto-PGE2. *Prostaglandins* **19,** 917–931 (1980).
49. Monkhouse, D. C., Van Campen, L. & Aguiar, a J. Kinetics of dehydration and isomerization of prostaglandins E 1 and E 2 . *J. Pharm. Sci.* **62,** 576–580 (1973).
50. Perera, S. K. & Fedor, L. R. Acid- and base-catalyzed dehydration of prostaglandin E2 to prostaglandin A2 and general-base-catalyzed isomerization of prostaglandin A2 to prostaglandin B2. *J. Am. Chem. Soc.* **101,** 7390–7393 (1979).
51. Grygiel-Górniak, B. Peroxisome proliferator-activated receptors and their ligands: nutritional and clinical implications--a review. *Nutr. J.* **13,** 17 (2014).
52. Naganuma, T., Sato, Y., Sassa, T., Ohno, Y. & Kihara, A. Biochemical characterization of the very long-chain fatty acid elongase ELOVL7. *FEBS Lett.* **585,** 3337–3341 (2011).
53. Campbell, W. B., Falck, J. R., Okita, J. R., Johnson, A. R. & Callahan, K. S. Synthesis of dihomoprostaglandins from adrenic acid acid) by human endothelial cells. **837,** 67–76 (1985).
54. Funk, C. D. Prostaglandins and leukotrienes: advances in eicosanoid biology. *Science* **294,** 1871–5 (2001).
55. Yokoyama, U., Iwatsubo, K., Umemura, M., Fujita, T. & Ishikawa, Y. The prostanoid EP4 receptor and its signaling pathway. *Pharmacol. Rev.* **65,** 1010–52 (2013).
56. Babaev, V. R. *et al.* Macrophage EP4 Deficiency Increases Apoptosis and Suppresses Early Atherosclerosis. *Cell Metab.* **8,** 492–501 (2008).
57. Ehrhardt, C. & Ludwig, S. A new player in a deadly game: influenza viruses and the PI3K/Akt signalling pathway. *Cell. Microbiol.* **11,** 863–871 (2009).
58. Coulombe, F. *et al.* Targeted prostaglandin E2 inhibition enhances antiviral immunity through induction of type I interferon and apoptosis in macrophages. *Immunity* **40,** 554–68 (2014).
59. Winau, F. *et al.* Apoptotic vesicles crossprime CD8 T cells and protect against tuberculosis. *Immunity* **24,** 105–17 (2006).
60. Phipps, R. P., Stein, S. H. & Roper, R. L. A new view of prostaglandin E regulation of the immune response. *Immunol. Today* **12,** 349–52 (1991).
61. Openshaw, P. J. M. & Tregoning, J. S. Immune Responses and Disease Enhancement during Respiratory Syncytial Virus Infection. *Clin. Microbiol. Rev.* **18,** 541–555 (2005).
62. Liu, Z. *et al.* Expression of 15-PGDH is downregulated by COX-2 in gastric cancer. *Carcinogenesis* **29,** 1219–27 (2008).
63. Otani, T. *et al.* Levels of NAD(+)-dependent 15-hydroxyprostaglandin dehydrogenase are reduced in inflammatory bowel disease: evidence for involvement of TNF-alpha. *Am. J. Physiol. Gastrointest. Liver Physiol.* **290,** G361–G368 (2006).
64. Lagadic-Gossmann, D., Huc, L. & Lecureur, V. Alterations of intracellular pH homeostasis in apoptosis: origins and roles. *Cell Death Differ.* **11,** 953–961 (2004).
65. Amici, C., Belardo, G., Rossi, A. & Santoro, M. G. Activation of I kappa b kinase by herpes simplex virus type 1. A novel target for anti-herpetic therapy. *J. Biol. Chem.* **276,** 28759–28766 (2001).
66. Santoro, M. G., Jaffe, B. M. & Esteban, M. Prostaglandin A inhibits the replication of vesicular stomatitis virus: Effect on virus glycoprotein. *J. Gen. Virol.* **64,** 2797–2801 (1983).
67. Storer, P. D., Xu, J., Chavis, J. A. & Drew, P. D. Cyclopentenone prostaglandins PGA2 and 15-deoxy-delta12,14 PGJ2 suppress activation of murine microglia and astrocytes: implications for multiple sclerosis. *J. Neurosci. Res.* **80,** 66–74 (2005).
68. de Marco, A. *et al.* Induction of the heat-shock response by antiviral prostaglandins in human cells infected with human immunodeficiency virus type 1. *Eur. J. Biochem.* **256,** 334–41 (1998).
69. Superti, F., Amici, C., Tinari, A., Donelli, G. & Santoro, M. G. Inhibition of rotavirus replication by

prostaglandin A: evidence for a block of virus maturation. *J. Infect. Dis.* **178,** 564–568 (1998).
70. Shu, J. Prostaglandin A(2) Blocks the Activation of G(1) Phase Cyclin-dependent Kinase without Altering Mitogen-activated Protein Kinase Stimulation. *J. Biol. Chem.* **271,** 9376–9383 (1996).
71. Yin, H. *et al.* Role of mitochondria in programmed cell death mediated by arachidonic acid-derived eicosanoids. *Mitochondrion* **13,** 209–24 (2013).
72. Davies, K. J. The broad spectrum of responses to oxidants in proliferating cells: a new paradigm for oxidative stress. *IUBMB Life* **48,** 41–7 (1999).
73. Reynaud, D., Thickitt, C. P. & Pace-Asciak, C. R. Facile preparation and structural determination of monohydroxy derivatives of docosahexaenoic acid (HDoHE) by alpha-tocopherol-directed autoxidation. *Anal. Biochem.* (1993).
74. VanRollins, M. & Murphy, R. C. Autooxidation of docosahexaenoic acid: analysis of ten isomers of hydroxydocosahexaenoate. *J. Lipid Res.* **25,** 507–517 (1984).
75. Le Faouder, P. *et al.* LC–MS/MS method for rapid and concomitant quantification of pro-inflammatory and pro-resolving polyunsaturated fatty acid metabolites. *J. Chromatogr. B* **932,** 123–133 (2013).
76. Kühn, H. & O'Donnell, V. B. Inflammation and immune regulation by 12/15-lipoxygenases. *Prog. Lipid Res.* **45,** 334–56 (2006).
77. Node, K. *et al.* Anti-inflammatory properties of cytochrome P450 epoxygenase-derived eicosanoids. *Science* **285,** 1276–1279 (1999).
78. Itoh, T. *et al.* Structural basis for the activation of PPARgamma by oxidized fatty acids. *Nat. Struct. Mol. Biol.* **15,** 924–31 (2008).

Chapter 4 Supplementary information

Supplementary Tables

Table S4.1: Descriptive statistics of the COX derived oxylipins. Metabolites are presented as their averaged normalised response and % RSD in brackets.

COX derived oxylipin metabolites	RSV						Mock						TNFa					
	0h	12h	24h	36h	48h	72h	0h	12h	24h	36h	48h	72h	0h	12h	24h	36h	48h	72h
PGF2a	0.07 (8.08)	0.3 (11)	0.9 (15.9)	2.33 (11.3)	8.06 (11.22)	18.12 (13.86	0.1 (7.66)	0.32 (8.29)	0.11 (56.91	0.09 (16.29)	0.07 (25.19)	0.1 (12.67)	0.1 (11.37)	0.15 (14.68)	0.37 (28.31)	0.38 (9.83)	0.37 (18)	0.73 (16.35)
13,14-dihydro-15-keto-PGF2a	0.02 (45.82)	0.17 (26.06)	0.55 (25.32)	1.13 (5.36)	3.73 (14.29)	9.07 (12.22)	0.04 (60.06)	0.12 (9.93)	0.08 (58.08	0.06 (8.34)	0.04 (42.95)	0.07 (13.98)	0.03 (19.88)	0.08 (21.7)	0.28 (37.44)	0.38 (6.6)	0.48 (19.85)	0.92 (10.53)
11beta-13,14-dihydro-15-keto-PGF2a	0.03 (23.09)	0.21 (17.47)	0.65 (26.99)	1.4 (7.78)	4.62 (21.97)	11.08 (8.28)	0.03 (20.83)	0.2 (7.22)	0.08 (18.3)	0.06 (19.45)	0.06 (11.12)	0.08 (4.47)	0.03 (23.57)	0.09 (21.23)	0.35 (23.55)	0.49 (18.67)	0.63 (17.99)	1.26 (10.94)
PGE2	0.05 (25.38)	0.52 (6.87)	1.41 (31.34)	5.19 (12.71	14.42 (9.68)	24.88 (12.37	0.08 (22.55)	0.31 (9.77)	0.08 (49.58	0.05 (40.16)	0.03 (22.3)	0.03 (15.29)	0.06 (21.59)	0.18 (20.41)	0.38 (26.2)	0.33 (15.48)	0.31 (14.71)	0.54 (13.81)
TXB2	0.21 (9.35)	0.32 (7.42)	0.49 (11.65)	1.07 (9.09)	3.57 (13)	7.94 (0.7)	0.33 (9.12)	0.59 (17)	0.23 (18.58	0.14 (9.56)	0.1 (15.21)	0.09 (8.64)	0.28 (16.28)	0.19 (14.69)	0.26 (10.11)	0.22 (17.5)	0.18 (22.19)	0.27 (27.78)
13,14-dihydro-15-keto-PGE2	0.02 (10.27)	0.15 (6.31)	0.3 (33.29)	0.52 (6.07)	0.93 (12.84)	0.94 (30.24)	0.02 (94.34)	0.08 (21.78	0.02 (23.39	0.01 (15.58)	0.01 (21.52)	0.01 (18.4)	0.02 (35.27)	0.07 (24.43)	0.14 (35.36)	0.15 (16.94)	0.14 (14.38)	0.21 (17.82)
Tetranor-PGEM	0.05 (15.13)	0.05 (26.21)	0.11 (13.03)	0.31 (19.45	0.84 (15.25)	1.91 (2.35)	0.1 (4.16)	0.16 (9.74)	0.04 (7.38)	0.02 (50.83)	0.01 (45.79)	0.01 (31.88)	0.06 (15.25)	0.04 (26.99)	0.11 (15.8)	0.1 (13.06)	0.08 (25.99)	0.08 (20.84)
PGF1a	nd	nd	0.1 (21.81)	0.32 (4.66)	1.47 (15.97)	3.74 (21.28)	nd	nd	nd	0.02 (89.79)	nd	nd	nd	0.03 (92.11)	nd	0.04 (93.04)	0.06 (18.32)	0.13 (16.3)
PGE1	0.01 (92.69)	0.01 (44.34)	0.01 (15.25)	0.1 (5.26)	0.37 (10.63)	0.71 (11.8)	nd	nd	nd	nd	nd	nd	nd	0.01 (108.82)	nd	0.01 (119.44)	0.01 (87.53)	0.01 (15.23)
1a,1b-dihomo-PGF2a	nd	0.02 (32.76)	0.05 (36.39)	0.17 (18.85	0.9 (14.41)	2.1 (11.51)	nd	nd	nd	nd	nd	nd	nd	nd	0.04 (90.55)	0.03 (70.38)	nd	0.04 (87.16)
bicyclo-PGE2	nd	0.04 (8.35)	0.06 (22.02)	0.13 (5.17)	0.33 (11.37)	0.98 (10.91)	nd	0.03 (23.82	0.01 (100.1	nd	nd	nd	nd	0.02 (47.98)	0.03 (15.32)	0.03 (19.97)	0.03 (24.55)	0.05 (16.24)
12S-HHTrE	0.13 (16.4)	0.02 (13.7)	0.02 (119.59	0.13 (42.2)	0.36 (22.76)	0.48 (12.95)	nd	0.02 (101.8	nd	nd	nd	nd	0.2 (20.09)	nd	nd	nd	nd	0.02 (56.31)
PGE3	nd	nd	0.01 (26.18)	0.06 (22.64	0.13 (10.97)	0.23 (20.99)	nd	nd	nd	nd	nd	nd	nd	nd	nd	nd	0.01 (14.19)	0.01 (12.59)
PGD2	0.01 (59.02)	0.04 (77.03)	0.04 (29.4)	0.15 (35.6)	0.48 (19.13)	0.66 (5.44)	0.02 (43.59)	0.06 (30.56	0.04 (121.5	0.04 (38.77)	0.02 (95.24)	0.01 (99.64)	0.01 (173.21)	0.03 (77.19)	0.02 (109.36)	0.02 (92.03)	0.01 (112)	0.05 (19.06)
PGA2	0.01 (46.2)	0.02 (35.8)	0.03 (14.47)	0.13 (19.9)	0.53 (5.12)	1.58 (14.46)	0.02 (88.99)	nd	nd	nd	nd	nd	0.01 (87.34)	0.01 (27.09)	0.02 (33.55)	0.01 (86.64)	0.01 (43.8)	0.01 (6.58)
15-keto-PGF2a	0.02 (38.76)	0.02 (20.25)	0.02 (92.9)	0.04 (87.5)	0.19 (34.51)	0.77 (7.95)	0.03 (27.41)	0.04 (30.28	nd	0.01 (88.28)	0.01 (68.83)	nd	0.05 (26.5)	0.01 (39)	0.02 (38.12)	0.02 (86.93)	nd	nd
LTB4	0.03 (100.29)	0.02 (92.73)	0.06 (57.29)	0.05 (46.31	0.15 (89.27)	0.28 (71.1)	0.02 (87.56)	0.04 (87.85	0.03 (95.12	0.03 (38.97)	0.02 (95.75)	0.02 (70.96)	0.06 (11.48)	0.02 (55.64)	0.03 (66.05)	0.02 (57.17)	0.01 (121.51)	0.02 (46.01)
d12-PGJ2	0.01 (37.32)	0.01 (21.25)	nd	0.02 (16.32	0.1 (24.08)	0.35 (4.53)	0.01 (89.04)	0.02 (25.97	0.02 (28)	0.01 (95.07)	0.01 (31.81)	0.01 (92.7)	0.02 (3.25)	0.01 (22.25)	0.01 (37.65)	0.01 (173.21)	nd	0.01 (54.9)
PGJ2	0.01 (33.49)	0.01 (25.98)	nd	0.03 (12.61	0.11 (23.84)	0.36 (7.34)	0.01 (89.09)	0.02 (27.15	0.02 (33.44	0.01 (88.79)	0.01 (24.25)	0.01 (55.79)	0.02 (6.06)	0.01 (33.08)	0.01 (29.97)	nd	nd	0.01 (46.17)
PGF3a	0.01 (101.95)	0.01 (74.38)	nd	0.01 (120.7	0.05 (57.86)	0.1 (12.19)	nd	0.01 (101.4	0.02 (81.98	0.01 (72.4)	0.01 (101.5)	0.01 (80.68)	0.01 (88.07)	0.01 (86.63)	0.01 (131.76)	0.01 (103.54)	0.01 (41.25)	nd

nd – Metabolites are not detected within at least 50% of the group.

Table S4.2: Descriptive statistics of the LOX derived oxylipins. Metabolites are presented as their averaged normalised response and % RSD in brackets.

LOX derived oxylipin metabolites	RSV						Mock						TNFa					
	0h	12h	24h	36h	48h	72h	0h	12h	24h	36h	48h	72h	0h	12h	24h	36h	48h	72h
5S,6S-Lipoxin A4	0.06 (43.32)	0.33 (15.29)	0.96 (32.23)	1.42 (11.41)	3.62 (11.06)	8.5 (5.63)	nd	0.76 (23.74)	0.59 (14.19)	0.58 (5.62)	0.46 (4.56)	0.51 (18.87)	0.09 (17.67)	0.25 (12.29)	0.54 (13.51)	0.49 (7.84)	0.55 (8.04)	0.75 (24.22)
9,10,13-TriHOME	0.07 (22.25)	0.14 (17.97)	0.22 (15.71)	0.3 (17.19)	0.72 (3.92)	2.05 (9.83)	0.14 (1.19)	0.29 (14.72)	0.16 (15.49)	0.13 (10.88)	0.11 (11.58)	0.11 (20.87)	0.11 (14.59)	0.08 (19.83)	0.16 (17.19)	0.11 (21.32)	0.1 (26.48)	0.09 (16.81)
12-HETE	0.95 (5.81)	0.54 (12.08)	0.31 (27.36)	0.3 (14.01)	0.83 (4.8)	3.25 (11.74)	1.88 (21.65)	1.04 (9.46)	0.24 (31)	0.1 (27.4)	0.06 (20.12)	0.06 (37.72)	1.47 (10.39)	0.21 (10.89)	0.1 (10.52)	0.06 (14.14)	0.04 (21.49)	0.05 (34.48)
15S-HETrE	0.33 (13.63)	0.41 (38.4)	0.35 (29.87)	0.5 (19.78)	2.24 (17.97)	8.58 (18.48)	0.66 (6.51)	0.67 (8.46)	0.21 (13.26)	0.15 (18.86)	0.09 (18.44)	0.06 (22.04)	0.49 (6.42)	0.15 (9.04)	0.14 (30.3)	0.11 (14.88)	0.08 (34.82)	0.07 (43.56)
8-HETrE	0.55 (6.7)	0.32 (4.13)	0.22 (34.45)	0.25 (18.54)	0.87 (5.05)	2.75 (8.31)	1.14 (21.53)	0.72 (34.46)	0.17 (25.34)	0.09 (32.32)	0.06 (15.95)	0.06 (22.86)	0.87 (19.2)	0.13 (20.35)	0.11 (50.07)	0.07 (42.19)	0.06 (20.18)	0.06 (9.82)
5-HETE	0.92 (6.48)	0.26 (21.39)	0.1 (64.1)	0.09 (37.49)	0.36 (7.94)	1.13 (41.5)	1.77 (14.83)	0.5 (6.79)	0.1 (52.14)	0.03 (9.89)	0.02 (53.19)	0.02 (49.14)	1.34 (11.28)	0.09 (24.12)	0.03 (16.06)	0.02 (87.32)	0.02 (39.32)	0.02 (59.93)
15-HETE	0.28 (18.05)	0.15 (43.74)	0.13 (20.05)	0.22 (26.93)	0.71 (25.17)	1.85 (22.04)	0.53 (10.69)	0.3 (5.8)	0.09 (35.59)	0.06 (23.73)	0.03 (25.37)	0.02 (35.62)	0.43 (20.58)	0.06 (20.77)	0.05 (42.24)	0.04 (4.08)	0.02 (14.92)	0.03 (11.99)
9,12,13-TriHOME	0.21 (4.26)	0.42 (21.72)	0.68 (23.98)	1 (25.95)	2.53 (13.95)	5.85 (8.54)	0.4 (11.38)	0.88 (16.34)	0.52 (10.97)	0.43 (31.05)	0.33 (18.42)	0.37 (25.11)	0.28 (11.32)	0.22 (16.34)	0.42 (9.74)	0.33 (9.87)	0.31 (6.42)	0.36 (12.26)
9-HODE	0.15 (14.16)	0.09 (22.55)	0.12 (24.65)	0.16 (40.59)	0.44 (14.76)	0.93 (10.58)	0.28 (4.12)	0.25 (27.45)	0.1 (15.09)	0.06 (17.96)	0.04 (15.78)	0.03 (12.81)	0.23 (15.9)	0.06 (37.88)	0.06 (40.84)	0.05 (12.51)	0.05 (8.29)	0.05 (10.84)
5S-HEPE	0.11 (19.87)	0.18 (30.43)	0.1 (65.26)	0.08 (22.58)	0.31 (27.89)	0.91 (3.92)	0.19 (19.36)	0.36 (6.02)	0.07 (42.08)	0.04 (56.5)	0.02 (27.9)	0.01 (33.43)	0.15 (13.98)	0.07 (29.76)	0.04 (8.38)	0.02 (11.42)	0.02 (37.28)	0.02 (31.06)
12S-HEPE	0.09 (22.7)	0.09 (14.63)	0.07 (15.4)	0.1 (12.21)	0.28 (22.12)	0.89 (27.42)	0.19 (22.14)	0.14 (23.17)	0.07 (23.51)	0.02 (92.41)	nd	nd	0.13 (7.01)	0.03 (19.05)	0.05 (43.32)	nd	nd	nd
15S-HEPE	0.02 (13.56)	0.06 (37.92)	0.05 (57.41)	0.09 (23.28)	0.3 (13.34)	0.78 (10.11)	0.05 (22.4)	0.11 (43.21)	0.04 (32.46)	0.02 (89)	0.02 (90.58)	0.02 (71.14)	0.05 (14.55)	0.03 (42.41)	nd	nd	0.01 (63.55)	0.01 (88.65)
9-HpODE	0.01 (86.86)	0.02 (37.19)	0.01 (106.53)	0.05 (42.29)	0.04 (87.39)	0.17 (90.07)	0.02 (110.01)	0.03 (16.55)	0.02 (19.11)	0.01 (47.47)	0.01 (94.82)	0.01 (96.8)	0.04 (41.63)	0.02 (41.62)	0.02 (8.48)	0.02 (93.77)	0.01 (108.82)	0.01 (40.44)
9-KODE	0.03 (14.26)	0.03 (78.58)	0.04 (81.71)	0.04 (63.2)	0.1 (64.97)	0.06 (123.54)	0.07 (33.95)	0.04 (25.75)	0.02 (69.28)	0.01 (10.69)	0.01 (34.67)	0.01 (26.18)	0.05 (38.85)	0.01 (38.06)	0.02 (36.33)	0.02 (9.86)	0.01 (28.77)	0.01 (42.78)
13-HODE	0.09 (11.09)	0.07 (12.51)	0.07 (27.08)	0.1 (25.79)	0.34 (13.84)	0.9 (10.97)	0.14 (21.53)	0.17 (11.28)	0.08 (26.86)	0.04 (23.09)	0.03 (33)	0.02 (37.74)	0.13 (12.71)	0.04 (24.17)	0.04 (41.2)	0.03 (31.02)	0.02 (36.35)	0.02 (28.77)
13-KODE	0.05 (19.41)	0.02 (102.8)	0.04 (15.04)	0.05 (21.71)	0.13 (37.39)	0.23 (14.95)	0.09 (13.32)	0.11 (13.96)	0.04 (19.77)	0.02 (32.95)	0.02 (42.64)	0.02 (35.91)	0.06 (28.88)	0.02 (34.66)	0.03 (12.79)	0.02 (19.78)	0.01 (45.04)	0.02 (39.2)

nd – Metabolites are not detected within at least 50% of the group.

Table S4.3: Descriptive statistics of the P450 derived oxylipins. Metabolites are presented as their averaged normalised response and % RSD in brackets.

P450 derived oxylipin metabolites	RSV						Mock						TNFa					
	0h	12h	24h	36h	48h	72h	0h	12h	24h	36h	48h	72h	0h	12h	24h	36h	48h	72h
11,12-DiHETrE	0.01 (118.06)	0.01 (27.11)	0.01 (19.39)	0.02 (4.31)	0.05 (20.58)	0.12 (19.6)	0.01 (35.71)	0.02 (16.52)	0.01 (11.89)	0.01 (47.24)	0.01 (19.94)	0.01 (22.06)	0.01 (10.57)	0.01 (14.76)	nd	0.01 (28.57)	0.01 (37.81)	0.01 (28.5)
14,15-DiHETrE	0.02 (40.36)	0.03 (12.26)	0.03 (34.72)	0.04 (11.27)	0.14 (8.36)	0.34 (13.03)	0.02 (13.6)	0.06 (31.14)	0.02 (18.5)	0.02 (23.9)	0.02 (8.66)	0.02 (34.5)	0.02 (17.4)	0.02 (14.35)	0.02 (38.67)	0.02 (16.27)	0.01 (15.01)	0.02 (9.18)
14,15-DiHETE	0.01 (40.66)	0.01 (114.4)	0.01 (93.41)	0.01 (43.47)	0.02 (100)	0.03 (88.86)	0.01 (95.77)	0.01 (90.7)	nd	nd	nd	0.01 (89.38)	0.01 (87.27)	0.01 (89.05)	nd	nd	nd	nd
17,18-DiHETE	0.05 (14.74)	0.06 (15.47)	0.05 (19.16)	0.08 (4.35)	0.18 (20.95)	0.34 (18.34)	0.08 (17.96)	0.13 (21.18)	0.05 (18.39)	0.02 (37.65)	0.02 (14.18)	0.01 (38.59)	0.08 (36.21)	0.04 (18.77)	0.03 (36.66)	0.01 (35.77)	0.01 (47.12)	0.01 (21.71)
19,20-EpDPE	0.23 (20.02)	0.1 (26.01)	0.03 (12.93)	nd	0.15 (48.05)	0.28 (23.85)	0.37 (9.89)	0.22 (29.23)	0.03 (101.44)	0.01 (87.38)	0.01 (33.96)	0.01 (134.92)	0.33 (20.89)	0.03 (10.9)	0.01 (89.47)	0.01 (92.1)	nd	nd
19,20-DiHDPA	0.02 (22.68)	0.02 (13.45)	0.03 (12.63)	0.03 (18.09)	0.1 (6.82)	0.26 (9.44)	0.03 (17.53)	0.05 (8.76)	0.02 (19.36)	0.01 (2.42)	0.01 (13.66)	0.01 (17.25)	0.03 (21.88)	0.02 (25.77)	0.01 (28.72)	0.01 (7.52)	0.01 (22.46)	0.01 (11.56)
9,10-EpOME	0.07 (30.44)	0.02 (90.82)	0.04 (15.99)	nd	0.07 (88.84)	nd	0.12 (21.32)	0.05 (93.85)	0.03 (95.74)	0.02 (33.86)	0.02 (40.65)	0.01 (173.21)	0.09 (12.85)	0.01 (104.79)	0.04 (33.87)	0.02 (88.93)	0.01 (93.24)	0.01 (110.16)
9,10-DiHOME	0.51 (3.37)	0.13 (16.15)	0.03 (32.23)	0.06 (43.94)	0.08 (26.3)	0.3 (41.73)	0.84 (10.24)	0.27 (1.34)	0.03 (23.07)	0.01 (46.27)	0.01 (87.73)	0.01 (100.83)	0.71 (4.55)	0.06 (16.65)	0.03 (49.64)	0.01 (51.11)	0.01 (88.72)	0.01 (51.89)
12,13-DiHOME	0.26 (10.33)	0.12 (29.22)	0.05 (37.34)	0.05 (53.08)	0.09 (40.49)	0.24 (50.63)	0.42 (4.38)	0.21 (19.78)	0.05 (28.5)	0.02 (24.5)	nd	0.01 (103.58)	0.34 (2.03)	0.06 (75.68)	0.03 (126.83)	0.01 (93.82)	nd	0.01 (20.28)

nd – Metabolites are not detected within at least 50% of the group.

Table S4.4: Descriptive statistics of the auto-oxidation (ROS) derived oxylipins. Metabolites are presented as their averaged normalised response and % RSD in brackets.

Auto-oxidation (ROS) metabolites	RSV						Mock						TNFa					
	0h	12h	24h	36h	48h	72h	0h	12h	24h	36h	48h	72h	0h	12h	24h	36h	48h	72h
9-HETE	0.04 (31.35)	0.02 (119.84)	0.01 (86.69)	nd	0.04 (89.73)	0.12 (6.45)	0.06 (22.59)	0.04 (87.43)	0.02 (89.94)	0.02 (49.88)	0.01 (18.48)	nd	0.06 (55.21)	nd	0.01 (43.38)	nd	nd	nd
4-HDoHE	0.88 (14.14)	0.39 (26.68)	0.08 (86.76)	nd	0.62 (44.34)	1.21 (92.53)	1.74 (18.41)	0.92 (14)	0.15 (88.94)	nd	0.03 (15.53)	nd	1.4 (11.14)	0.12 (7.7)	0.05 (89.21)	nd	nd	nd
14-HDoHE	0.16 (17.15)	0.09 (11.19)	0.08 (72.53)	0.13 (39.16)	0.37 (30.48)	1.03 (19.9)	0.36 (19.63)	0.26 (18.94)	0.08 (16.94)	0.04 (58.27)	0.02 (42.42)	0.03 (40.57)	0.28 (21.57)	0.06 (8.17)	0.04 (38.48)	0.02 (46.29)	0.01 (59.51)	0.02 (46.62)
10-HDoHE	0.2 (33.59)	0.12 (21.58)	0.08 (28.14)	0.12 (28.78)	0.36 (3.6)	1.22 (2.79)	0.34 (16.85)	0.22 (18.85)	0.07 (54.14)	0.03 (35.8)	0.02 (65.14)	0.03 (54.81)	0.29 (11.06)	0.06 (15.13)	0.05 (17.83)	0.03 (57.55)	0.02 (33.56)	0.02 (26.04)
11-HDoHE	0.33 (12.21)	0.28 (23.48)	0.22 (28.3)	0.26 (17.6)	0.73 (13.65)	2.87 (27.68)	0.63 (34.76)	0.51 (25.6)	0.15 (30.25)	0.09 (20.67)	0.07 (18.86)	0.04 (53.39)	0.48 (11.34)	0.13 (13.72)	0.11 (20.09)	0.05 (23.53)	0.05 (7.82)	0.04 (22.47)
11-HETE	0.52 (7.2)	0.34 (17.56)	0.29 (32.75)	0.75 (34.44)	2.09 (9.19)	5.8 (9.5)	0.98 (25.65)	0.7 (22.65)	0.19 (37.02)	0.09 (20.04)	0.08 (15.23)	0.05 (44)	0.74 (4.55)	0.15 (18.19)	0.12 (8.45)	0.09 (4)	0.09 (26.04)	0.12 (21.98)
13-HDoHE	0.48 (22.75)	0.32 (34.92)	0.25 (43.7)	0.31 (18.63)	1.15 (8.35)	3.49 (6.52)	0.9 (21.88)	0.77 (5.27)	0.21 (29.65)	0.12 (23.16)	0.07 (9.56)	0.06 (32.4)	0.64 (10.03)	0.15 (22.75)	0.15 (25.13)	0.09 (36)	0.05 (30.75)	0.06 (23.77)
16-HDoHE	0.44 (11.18)	0.37 (13.02)	0.42 (39.79)	0.57 (10.85)	1.65 (7.7)	4.76 (10.15)	0.83 (20.47)	0.88 (28.75)	0.32 (22.59)	0.17 (8.02)	0.11 (40.23)	0.08 (18.63)	0.68 (5.54)	0.2 (11.41)	0.18 (13.31)	0.11 (2.18)	0.08 (13.75)	0.07 (34.36)
17-HDoHE	0.23 (10.48)	0.17 (4.44)	0.14 (89.99)	0.55 (15.41)	1.91 (13.39)	4.58 (14.24)	0.54 (35.26)	0.26 (26.8)	0.15 (17.89)	0.03 (87.13)	0.03 (48.1)	0.04 (35.85)	0.29 (2.33)	0.09 (6.24)	0.06 (106.05)	0.08 (21.37)	0.05 (102.09)	0.15 (24.04)
18-HEPE	0.06 (7.55)	0.15 (10.57)	0.27 (25.04)	0.32 (14.83)	0.96 (11.66)	2.7 (18.24)	0.1 (7.42)	0.32 (26.09)	0.17 (9.77)	0.1 (22.44)	0.07 (9.91)	0.05 (23.73)	0.07 (19.55)	0.09 (9.87)	0.09 (3.79)	0.07 (13.33)	0.05 (11.86)	0.05 (8.58)
20-HDoHE	0.33 (14.09)	0.35 (13.14)	0.43 (21.18)	0.49 (18.08)	1.47 (8.4)	3.66 (14.17)	0.49 (39.92)	0.65 (21.78)	0.22 (12.37)	0.14 (24.41)	0.07 (4.97)	0.07 (46.42)	0.41 (9.49)	0.17 (3.44)	0.16 (27.87)	0.09 (62.09)	0.06 (15.43)	0.06 (29.62)
5-iPF2a-VI	0.03 (48.33)	0.05 (22.6)	0.11 (17.73)	0.2 (9.35)	0.68 (4.24)	1.51 (5.33)	0.03 (9.07)	0.12 (28.43)	0.09 (13.74)	0.08 (12.7)	0.07 (15.48)	0.07 (24.3)	0.02 (61.24)	0.04 (23.54)	0.07 (28.63)	0.06 (4.81)	0.06 (14.18)	0.11 (15.65)
7-HDoHE	0.24 (7.23)	0.17 (26.71)	0.16 (33.92)	0.17 (11.6)	0.51 (24.49)	2.22 (29.84)	0.48 (27.49)	0.43 (20.54)	0.15 (20.3)	0.07 (14.95)	0.04 (20.36)	0.03 (42.55)	0.4 (4.89)	0.09 (21.05)	0.07 (7.91)	0.05 (16.31)	0.04 (39.84)	0.04 (33.09)
8_HDoHE	0.33 (18.06)	0.3 (17.34)	0.21 (34.7)	0.21 (22.53)	0.86 (13.96)	3.13 (7.21)	0.54 (11.95)	0.57 (19.43)	0.16 (34.03)	0.07 (26.1)	0.04 (9.02)	0.04 (34.37)	0.38 (3.98)	0.12 (10.54)	0.1 (26.96)	0.06 (25.65)	0.05 (63.9)	0.06 (39.21)
8-HETE	0.13 (19.96)	0.16 (43.38)	0.09 (18.33)	0.1 (64.62)	0.29 (25.57)	1.23 (23.8)	0.28 (27.16)	0.38 (19.98)	0.11 (59.94)	0.06 (22.21)	0.02 (86.62)	0.02 (86.74)	0.18 (24.11)	0.08 (19.68)	0.05 (39.55)	0.01 (86.62)	0.03 (24.73)	0.02 (41.49)

nd – Metabolites are not detected within at least 50% of the group.

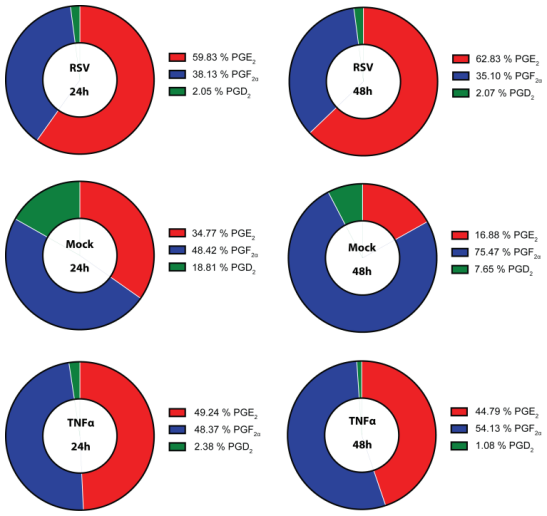

Figure S4.1: Visualisation of the ratio of the three main prostaglandins PGE_2, $PGF_{2\alpha}$, and PGD_2. Inspecting the 48h ratio for the RSV group indicate an almost 2/3 majority for PGE_2. For the Mock infection group $PGF_{2\alpha}$ has a ¾ majority. Lastly looking at the positive TNFα control group almost equal levels of $PGF_{2\alpha}$ and PGE_2 were found. In all three groups PGD_2 was the least synthesised prostaglandin.

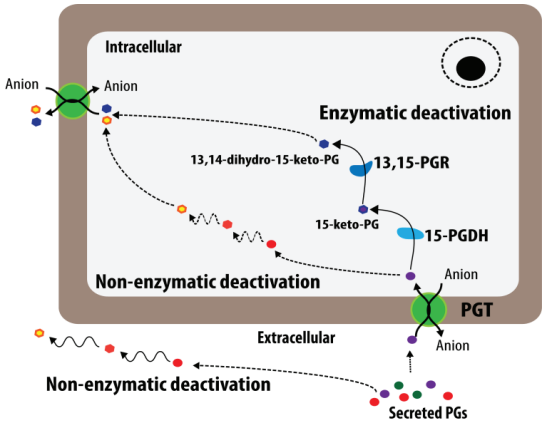

Figure S4.2: Prostaglandin deactivation and catabolism. In the extracellular space PGs are absorpt via the PGT into the cell where enzymatically deactivation takes place. PGs are deactivated and metabolise via 15-PGHD and 13,15-PGR to a metabolic inert downstream metabolite. Spontaneous non-enzymatic deactivation can also take place especially for PGE and PGD series metabolites. PGT: Prostaglandin transporter, 15-PGDH: 15-hydroxyprostaglandin dehydrogenase, 13,15-PGR : Δ13-15-ketoprostaglandin reductase.